Tellus (1998), 50A, 451–467
Printed in UK – all rights reserved

TELLUS
ISSN 0280–6495

On the estimation of transport characteristics of atmospheric data sets

By ARNE M. BRATSETH, *Department of Geophysics, University of Oslo, P.O. Box 1022, Blindern, 0315 Oslo 3, Norway*

(Manuscript received 24 September 1997; in final form 13 May 1998)

ABSTRACT

Transport characteristics of an atmospheric general circulation model have been estimated by analysing 30 000 trajectories over several months. These trajectories have been used to construct an advection-diffusion operator for the zonally-averaged transport of passive tracers. Several different methods have been tried for this purpose. The most promising seems to be a method where eddy-flux statistics for a large number of tracers are generated and used to find an optimized flux-gradient relationship. An alternative approach based on Lagrangian averaging is shown to be much less robust with respect to changes in the details of the procedure. The meridional circulation of the advection-diffusion operator is direct almost everywhere, but is very weak outside the tropics. Diffusion coefficients show a quite complicated structure with minima near the jet maxima. Certain limitations of the advection-diffusion model have been identified. In particular, there seems to be problems related to Walker cells. The use of a large number of different tracers has also allowed us to improve on the flux-gradient relationship by including higher order terms. The relevance of the advection-diffusion approach for the transport of potential vorticity has been tested. The Stokes drift is shown to be very important for potential vorticity fluxes near the tropopause.

1. Introduction

Averaging in time or space of data sets from real or simulated atmospheres is often necessary in order to reduce the amount of information to a more manageable level. In this process, however, information which is essential for a deeper understanding of the system, is often lost. In particular a reliable picture of the average motion of the air is difficult to obtain. This represents a serious problem since the effect of air moving from one place to another is of basic importance to the transport of momentum, energy, water vapour, pollutants etc. A thorough knowledge of the average advective transport, or average kinematics of the atmosphere, ought to be essential both for theoretical progress, and for use in all sorts of simplified models where eddies are parameterized.

In this work, we have tried to compute zonal and time averaged properties of a large set of trajectories generated by a GCM. This task is connected with important conceptual problems. It seems natural to try to model the average advective transport by means of some kind of mean flow, together with stochastic modelling of the effect of departures from this flow. However, in the general case this mean flow cannot be constructed from velocities averaged in the usual Eulerian way. The eddies may produce so called "Stokes' drift" phenomena which represent systematic contributions to the average advective transport. The impact of this effect has been demonstrated in GCM-experiments by Kida

e-mail: arne.bratseth@geofysikk.uio.no

(1977) and Kida (1983). Theoretical discussions of the effect are given by Plumb (1979) and Matsuno (1980).

Modelling of the average effect of departures from the mean flow is also a non-trivial problem. A diffusion model represents a natural first choice. However, this approach does not cover all the types of phenomena that may occur, and should only be considered as a first approximation to this part of the advective transport.

The main approach followed in this work is to compute an advection-diffusion operator with transport characteristics as close as possible to the average advective transport of the complete data set. Plumb and Mahlmann (1987) attacked this problem by computing a flux-gradient relation based on 2 tracers. We have extended this approach by optimizing results for a large number of tracers. The tracer statistics is generated directly from the trajectories. The large number of tracers used, makes it possible to discuss the limitations of the advection-diffusion approach, and allows us to extend the model by including more terms. We have also compared these results to a more direct approach based on Lagrangian averaging along the trajectories. In this process we have tried to shed some light on conceptual problems related to Lagrangian mean velocities. Finally we have studied the extent to which the flux of potential vorticity can be captured by the flux-gradient model.

2. The flux-gradient relation

A conserved constituent with mixing ratio q satisfies the averaged continuity equation:

$$\frac{\partial \overline{\rho q}}{\partial t} = -\nabla \cdot \overline{\rho q \boldsymbol{v}} \tag{1}$$

where ρ is air density, $\boldsymbol{v}$ is velocity, and the overbar represents an average which we do not need to specify at this stage.

We shall now try to model the flux-divergence in (1) as the result of a mean advection with a velocity $\boldsymbol{v}_{\mathrm{T}}$ combined with diffusion specified by a tensor $\boldsymbol{D}$. For simplicity, we shall assume that the density can be taken outside all averages, and is independent of time. Then we have:

$$\rho \frac{\partial \overline{q}}{\partial t} = -\nabla \cdot (\rho \overline{q} \boldsymbol{v}_{\mathrm{T}}) + \nabla \cdot (\rho \boldsymbol{D} \cdot \nabla \overline{q}) + \cdots, \tag{2}$$

where the dots indicate effects that cannot be described by advection or diffusion. The transport velocity $\boldsymbol{v}_{\mathrm{T}}$ and the diffusion tensor $\boldsymbol{D}$ are assumed to be properties of the flow itself, and should be independent of the tracer q. The advection and diffusion terms in (2) have simple physical interpretations. If we can find an operator of this kind which provides a good fit for arbitrarily chosen tracers, it will be of great help in analysing what the fluid is doing on average.

This advection-diffusion formulation is equivalent to a flux-gradient assumption for the eddy-flux:

$$\rho \overline{q' \boldsymbol{v}'} = \rho \overline{q \boldsymbol{v}} - \rho \overline{q} \overline{\boldsymbol{v}} = -\rho \boldsymbol{K} \cdot \nabla \overline{q}. \tag{3}$$

Notice that the expression for the eddy-flux should vanish when q is a constant, and therefore should not contain a zero order term proportional to $\overline{q}$. This, however, does not mean that the transport velocity in (2) has to be equal to $\overline{\boldsymbol{v}}$. It is convenient to consider the tensor $\boldsymbol{K}$ to be a sum of two parts, a symmetric part:

$$\boldsymbol{D} = \tfrac{1}{2}(\boldsymbol{K} + \boldsymbol{K}^{\mathrm{T}}), \tag{4}$$

and an anti-symmetric part:

$$\boldsymbol{L} = \tfrac{1}{2}(\boldsymbol{K} - \boldsymbol{K}^{\mathrm{T}}), \tag{5}$$

where the superscript T represents the transpose. Plumb (1979) and Matsuno (1980) have shown that the anti-symmetric part represents mean advection rather than diffusion. The flux due to $\boldsymbol{L}$ can always be reformulated as:

$$-\rho \boldsymbol{L} \cdot \nabla \overline{q} = \boldsymbol{b} \times \nabla \overline{q} \tag{6}$$

where the vector $\boldsymbol{b} = \rho(\boldsymbol{L}_{23}, -\boldsymbol{L}_{13}, \boldsymbol{L}_{12})$ is defined by the components of $\boldsymbol{L}$. If we introduce a new vector:

$$\boldsymbol{v}_{\mathrm{D}} = \rho^{-1} \nabla \times \boldsymbol{b}, \tag{7}$$

we can reformulate (6) as:

$$-\rho \boldsymbol{L} \cdot \nabla \overline{q} = \rho \overline{q} \boldsymbol{v}_{\mathrm{D}} - \nabla \times \overline{q} \boldsymbol{b}. \tag{8}$$

The last term in (8) is non-divergent so that:

$$-\nabla \cdot (\rho \boldsymbol{L} \cdot \nabla \overline{q}) = \nabla \cdot (\rho \overline{q} \boldsymbol{v}_{\mathrm{D}}), \tag{9}$$

indicating the advective nature of this part of the eddy-flux. The transport velocity in (2) is then identified as $\boldsymbol{v}_{\mathrm{T}} = \overline{\boldsymbol{v}} + \boldsymbol{v}_{\mathrm{D}}$. Notice that $\boldsymbol{v}_{\mathrm{D}}$ is mass-conserving by definition. Plumb (1979) has shown that for small amplitude waves $\boldsymbol{v}_{\mathrm{D}}$ is related to the Stokes' drift, so that $\boldsymbol{v}_{\mathrm{T}}$ is related to the Lagrangian

mean velocity as defined by Andrews and McIntyre (1978). However, the Stokes' drift and the Lagrangian mean velocity also contain other contributions, and are divergent in the general case.

The symmetric tensor $\boldsymbol{D}$ can be expected to describe mixing and random processes. However, this interpretation requires positive eigenvalues. Negative eigenvalues would mean that there are directions with anti-diffusion; a situation which is not easy to interpret.

In the following we shall let the bar represent a combined zonal and time average, so that the problem becomes 2-dimensional. Notice, however, that the formalism of this section also applies to 3-dimensional problems.

3. Computational approach

3.1. Solving for K

Plumb and Mahlman (1987) studied the zonally averaged transport characteristics of a general circulation model by computing the tensor $\boldsymbol{K}$ from tracer experiments. If the bar represents a combined zonal and time average, each tracer provides us with two equations:

$$\overline{q'v'} = -K_{yy}\frac{\partial \overline{q}}{\partial y} - K_{yz}\frac{\partial \overline{q}}{\partial z}, \tag{10}$$

$$\overline{q'w'} = -K_{zy}\frac{\partial \overline{q}}{\partial y} - K_{zz}\frac{\partial \overline{q}}{\partial z}. \tag{11}$$

If flux and gradient statistics is generated for 2 tracers, we have four equations which can be solved for the four components of $\boldsymbol{K}$ provided that the gradients of the tracers do not coincide in direction. This approach was used by Plumb and Mahlman (1987).

With only 2 tracers, however, it is not clear to what extent the results are independent of the tracers chosen. As an alternative we suggest to use statistics for a large number of tracers, and to find the tensor $\boldsymbol{K}$ which minimizes weighted sums of squared errors:

$$J_v = \sum_i W_{vi}\left(\overline{q_i'v'} + K_{yy}\frac{\partial \overline{q_i}}{\partial y} + K_{yz}\frac{\partial \overline{q_i}}{\partial z}\right)^2, \tag{12}$$

$$J_w = \sum_i W_{wi}\left(\overline{q_i'w'} + K_{zy}\frac{\partial \overline{q_i}}{\partial y} + K_{zz}\frac{\partial \overline{q_i}}{\partial z}\right)^2. \tag{13}$$

In order to make the contributions from different tracers comparable, we have chosen to use the weights:

$$W_{vi} = \langle(\overline{q_i'v'})^2\rangle^{-1}, \tag{14}$$

$$W_{wi} = \langle(\overline{q_i'w'})^2\rangle^{-1}, \tag{15}$$

where $\langle\ \rangle$ represents a mass-weighted average over the whole atmosphere. Minimizing (12) and (13) we get linear equations which are as easy to solve as (10) and (11). In the actual calculations we have used the meridional coordinate $y = a\phi$ where ϕ is latitude and a is the radius of the earth, and the logarithmic pressure coordinate $z = H\ln(p_0/p)$ with $H = 8000$ m and $p_0 = 1000$ hPa.

If the tracers are perfectly conserved they will be completely mixed, their gradients will vanish, and we will be unable to solve for $\boldsymbol{K}$. In order to maintain some gradients we have relaxed the tracers towards prescribed profiles $\hat{q}(y, z)$ by means of:

$$\frac{dq}{dt} = -\frac{1}{\tau}(q - \hat{q}). \tag{16}$$

Unlike Plumb and Mahlman (1987) we have chosen to let the relaxation time τ be constant in space.

3.2. GCM data set

The data set that has been studied was generated by a version of the ECMWF-model. The version is the cycle 36 with horizontal resolution T21 and 19 vertical levels. This model was run for 6 months with a constant January forcing. The state of this model-atmosphere was stored at intervals of 6 h. The data were interpolated to 15 pressure surfaces (1000 hPa, 900 hPa, 800 hPa, 700 hPa, 600 hPa, 500 hPa, 400 hPa, 300 hPa, 250 hPa, 200 hPa, 150 hPa, 100 hPa, 70 hPa, 50 hPa and 30 hPa), and to a longitude-latitude grid with ($\Delta\lambda = \Delta\phi = 5.625^\circ$.

Due to its low horizontal resolution this GCM cannot be expected to produce a particularly good simulation by current standards (Tibaldi et al., 1990). Our main objective, however, is to study methodological problems, and for this purpose this relatively small data set has proved to be convenient.

3.3. Trajectories

We have chosen to perform the tracer calculations by means of trajectories. For the last 5 months of this data set we have computed 3-dimensional trajectories for 30 000 particles. Initially the particles are distributed uniformly with respect to mass, i.e., with a density proportional to the air-density. The trajectories are computed from horizontal and vertical velocities which have been interpolated linearly in time to give a resolution of $\Delta t = 1$ h. The position at the time t_{n+1} of a particle with the position $\boldsymbol{x}_n$ at time t_n is calculated by the two-step procedure:

$$\boldsymbol{x}'_{n+1/2} = \boldsymbol{x}_n + \boldsymbol{v}(\boldsymbol{x}_n, t_{n+1/2})\frac{\Delta t}{2}, \tag{17}$$

$$\boldsymbol{x}_{n+1} = \boldsymbol{x}_n + \boldsymbol{v}(\boldsymbol{x}'_{n+1/2}, t_{n+1/2})\Delta t. \tag{18}$$

Velocities and positions are represented in spherical coordinates. These coordinates require special attention close to the poles because the horizontal velocity components will vary strongly over short distances even if the velocity vector itself is nearly constant. For this reason we have chosen to shift to a polar stereographic coordinate system whenever the starting point of a trajectory is polewards of $\pm 70^\circ$. The velocity components are interpolated from the closest grid points by repeated linear operations in λ, ϕ, and p. The particle positions together with the interpolated particle velocities are stored once a day.

The particle density was initially roughly proportional to the air density, and ought to remain so at all times. The integration procedure seems to take care of this in most places, but certain problems have been encountered near the top (30 hPa) and bottom (1000 hPa) of the integration volume. Since we do not have velocity data outside these boundaries, we have chosen not to allow particles to leave this volume even when the vertical velocity say that they should. This artificial device causes a certain accumulation of particles in some gridboxes, and dilution in others, especially at the top. In order to correct for this we have implemented a simple procedure. By the end of each day we count the number of particles in each latitude circle of gridboxes both in the top and bottom layer. For each of the 2 layers we identify the gridbox circle with highest and lowest particle number relative to the mass of the circle. A randomly chosen particle is then moved from the most crowded to the least crowded circle by simply changing its latitude coordinate. The procedure is repeated five times for both top and bottom before time integration is restarted. Thus a total of 10 trajectories are terminated and 10 new trajectories are initiated each day. This procedure seems to provide a reasonably homogeneous distribution of the particles.

3.4. Tracer calculation

The trajectories provides us with a simple and efficient way of generating the necessary tracer statistics at grid points. We have used a 2-dimensional grid in latitude and pressure, based on the grid that was defined above for the velocity data. The particle positions have been stored in a way which allows us to analyse the trajectories one by one. The tracer eq. (16) are integrated along the trajectories by means of a simple forward integration with time steps of one day. The profiles $\hat{q}$ defined below, are used as initial values. For each time step, the quantities that we need are calculated at the trajectory point, and are then transferred to the closest grid point. At the grid points sums are accumulated for each quantity. When all the trajectories have been scanned in this way we can calculate the statistics for each grid point from formulas like:

$$\overline{q\boldsymbol{v}} = \frac{\sum_i \sum_j a_{i,j} q_{i,j} \boldsymbol{v}_{i,j}}{\sum_i \sum_j a_{i,j}}, \tag{19}$$

where the subscript i refers to time, the subscript j refers to the trajectory, and $a_{i,j}$ is a weighting factor which is equal to one when the grid point happens to be the closest to the particle, and zero otherwise.

Note that the procedure described above will only be useful if each grid box is visited sufficiently often. There will certainly be moments when some grid points are not influenced by any particle. This would be a serious problem if we wanted to produce instantaneous fields, but we are only interested in fields that are averaged over longer time periods, and for this purpose the method seems to be adequate. We have monitored the sum $\Sigma_i \Sigma_j a_{i,j}$ divided by the gridbox mass, and it shows a reasonably uniform distribution in space. For consistency we have used this procedure for all quantities that are needed, even for $\overline{v}$ which

can also be computed from the gridded data. A comparison of the two versions of $\bar{v}$ shows only minor differences. The natural alternative to this approach would be to integrate the tracer fields by means of some kind of Eulerian transport model. This, however, would be far more expensive in terms of computer time. With our procedure the most time consuming part of the calculation is the construction of the trajectories which are independent of the tracers. The extra computer time connected to each tracer is small in comparison. Thus the cost of a large number of tracers is not much higher than the cost of one. This also applies to storage. Because the tracers are integrated along one trajectory at the time, they are never stored as 3-dimensional fields, only as 2-dimensional time and zonal averages. A disadvantage of the method is the smoothing which inevitably follows from the primitive interpolation to grid points. These errors, however, should be seen in relation to the very considerable errors of most Eulerian advection schemes.

3.5. *Defining the tracers*

The functions $\hat{q}$ in (16) are defined by means of Chebyshev polynomials. Standard textbooks on numerical analysis define the Chebyshev polynomial of order n by the recursive formula:

$$T_n(x) = 2xT_{n-1}(x) - T_{n-2}(x), \tag{20}$$

with $T_0(x) = 1$ and $T_1(x) = x$. Inside the interval $[-1, 1]$ these polynomials show a relatively homogeneous wavelike behaviour with n zero points so that different values of n represent different scales. They are chosen because of their computational convenience, and because they include the linear function. A set of functions are defined by:

$$\hat{q}_{m,n}(y, z) = T_m\left(\frac{y}{y_{\max}}\right) T_n\left(\frac{z - z_m}{z_m}\right), \tag{21}$$

where $y_{\max}$ is the coordinate of the north-pole, and z_m is the mean height of the part of the atmosphere that we are studying. With m and n ranging from 0 to 9 we have generated 99 different tracers. (The constant $\hat{q}_{0,0}$ is of course useless.)

4. Results

4.1. *Basic experiment, 99 tracers, $\tau = 30$ days*

As our basic experiment we have used all the 99 tracers and a relaxation time $\tau = 30$ days in (16). The symmetric diffusion tensor $\boldsymbol{D}$ is shown in Fig. 1a, b and c. The components D_{yy} (Fig. 1a) and D_{zz} (Fig. 1b) are positive almost everywhere, and the negative values (shaded) that occur are very small. Due to the symmetry we can always find a rotated coordinate system in which the tensor becomes diagonal. Each cross in Fig. 1c shows the orientation of this local coordinate

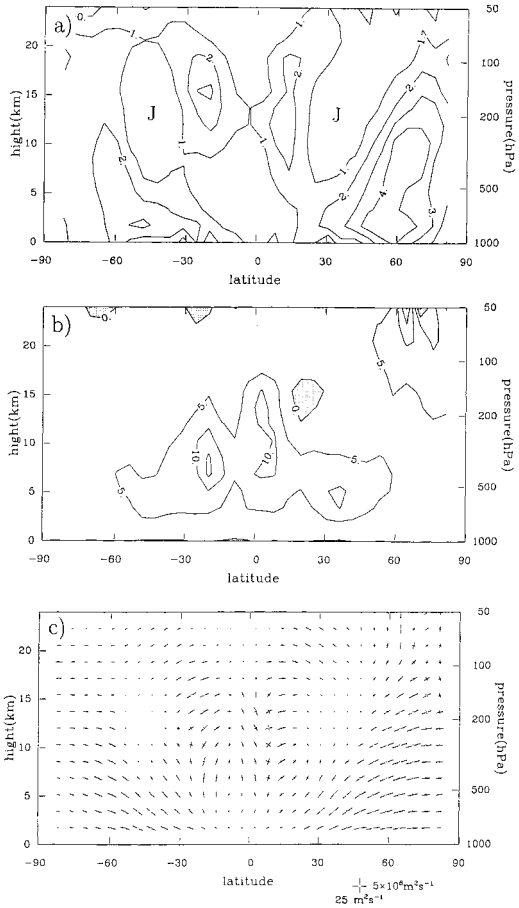

Fig. 1. The tensor $\boldsymbol{D}$ *for the basic experiment with* 99 *tracers and* $\tau = 30$ days. (a) D_{yy}, units 10^6 m^2 s^{-1}. (b) D_{zz}, units 1 m^2 s^{-1}. (c) Total tensor, magnitude indicated by reference cross near lower right corner, see text for explanation.

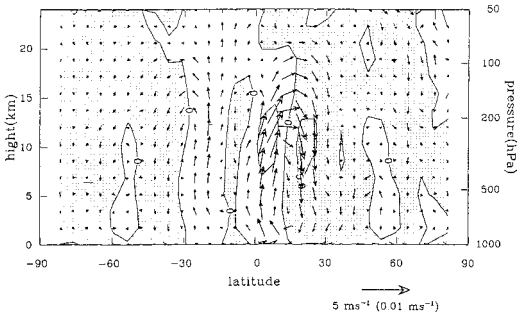

Fig. 2. Transport velocity $\boldsymbol{v}_T$ for the basic experiment with 99 tracers and $\tau = 30$ days. Reference vector 5 ms^{-1} as horizontal, 0.01 ms^{-1} as vertical. Isolines: vertical component w_T, interval 0.005 ms^{-1}, negative values are shaded.

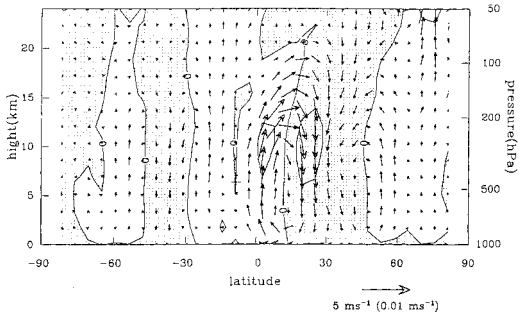

Fig. 3. As Fig. 2 but Eulerian mean meridional velocity $\bar{\boldsymbol{v}}$.

system, and the length of each cross-bar is proportional to the corresponding diffusion coefficient. A few negative values have been set to zero. The crosses give some idea about the behaviour of a cloud of particles diffusing from each point. Notice, however, that the size of such a cloud will grow like $(Dt)^{1/2}$, and therefore the crosses do not show the shape of the clouds directly. As in Plumb and Mahlman (1987) the diffusion shows a strong tendency to be oriented along isentropic surfaces.

Fig. 1 shows that the diffusion coefficient D_{yy} varies by more than one order of magnitude. Extremely small values are found in the jet stream areas (indicated by J in Fig. 1a), while the largest values are found in the troposphere beneath and poleward of the jet streams. There are also large values in two bands equatorward of the two jet streams. These bands seem to extend into the stratosphere. Inspection of the eddy kinetic energy has shown that the weak mixing in the jet stream regions is not due to any lack of eddy activity. We believe that the phenomenon is due to structural properties of the eddies, not their strength or frequency. Irreversible wave-breaking tend to take place on the sides of the jet rather than in the centre where the air is passing through the weather systems at a high speed.

Fig. 2 shows the transport velocity $\boldsymbol{v}_T$. For comparison $\bar{\boldsymbol{v}}$ is shown in Fig. 3. The isolines in these figures show the vertical velocity components w_T and $\bar{w}$ with negative values shaded. In addition to the strong winter Hadley cell and the much weaker summer Hadley cell, Fig. 3 also shows two well defined indirect Ferrel cells. These indirect circulations are not found in Fig. 2. Instead the transport velocity shows direct circulation over most of the extratropics. This circulation, however, is very weak. In the tropics the transport velocity is relatively similar to the Eulerian mean velocity.

Many of these features are also found in the results of Plumb and Mahlman (1987). Note, however, that they have used the meridional coordinate $y = a \sin \phi$ which means that their horizontal diffusion coefficients contain a factor $\cos^2 \phi$ relative to ours. Even when this has been accounted for it seems that our values for D_{yy} are considerably larger in much of the extratropical troposphere. Another feature which seems to be different is related to the vertical diffusion coefficient. Plumb and Mahlman (1987) report a maximum of 60 $m^2 s^{-1}$ in the upper tropical troposphere. Our results also show maxima at high levels in low latitudes, but the values are not larger than 16 $m^2 s^{-1}$. The transport velocity of Plumb and Mahlman (1987) is similar to ours in that it mainly consists of two direct circulation cells.

These two studies have used different GCMs, and this could certainly explain the differences pointed out above. However, we should also consider the possibility that some differences may be due to differences in the method used to analyse the data. We have made a number of experiments in order to study the sensitivity of our method to changes in various details.

4.2. *Two tracers, $\tau = 30$ days*

We have repeated the experiment above with only 2 tracers generated by relaxation towards

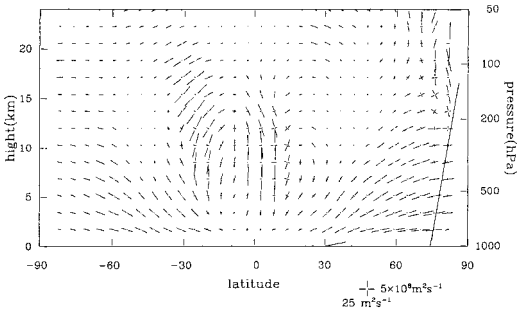

Fig. 4. As Fig. 1c but for the experiment with 2 tracers and $\tau = 30$ days.

$\hat{q}_{1,0} = y/y_{\max}$ and $\hat{q}_{0,1} = (z - z_m)/z_m$). Fig. 4 shows the diffusion tensor. Due to a boundary problem the method breaks down at the upper level near the North pole. A closer look at the trajectories in this area shows strong wave motions which tend to extend outside our analysis area. Clearly no method can analyse the transport characteristics of a truncated motion system, and we should therefore disregard this area. In most other places the results are qualitatively similar to the basic experiment, but the values tend to be larger. The coefficient D_{yy} has been increased by 30%–50%, while D_{zz} is about three times as big in the tropical maxima. The transport velocity (not shown) did not change much from the basic experiment, but there were some significant differences especially at high levels in the tropics.

Although 2 tracers seem to be insufficient, it may not be necessary to use as many as 99. Experiments with smaller subsets of tracers have shown that one can do quite well with the basic tracers of the form $\hat{q}_{m,0}$ and $q_{0,n}$. Tracer profiles which are products of these functions do not add much new information. Furthermore it is not necessary to use all values of m and n. In fact results for the set of five tracers $q_{1,0}$, $q_{3,0}$, $q_{0,1}$, $q_{0,3}$, $q_{0,7}$ are much closer to the case with 99 tracers than to the case with two. With fewer tracers, however, the agreement with the basic experiment quickly deteriorates.

4.3. *Sensitivity to* τ

The sensitivity with respect to the relaxation time τ was studied by repeating the two experiments described above with $\tau = 10$ days and $\tau = 90$ days. The experiments with 99 tracers show very little dependence on this parameter. The figures are not shown because they are practically indistinguishable from Figs. 1 and 2. With 2 tracers, however, the sensitivity is strong. In general the diffusion coefficients tend to increase with increasing τ. This tendency is particularly strong for D_{zz} in the tropics. For τ equal to 10, 30 and 90 days the maximum values are 30, 54, and 90 $\mathrm{m^2\,s^{-1}}$ respectively. The corresponding values for the experiments with 99 tracers are 13, 16, and 16 $\mathrm{m^2\,s^{-1}}$. Again the transport velocity does not seem to be very sensitive. As one would expect, with 2 tracers both the transport velocity and the diffusion coefficients become more noisy when the relaxation time is increased.

The low sensitivity of the results for the full set of tracers suggests that it may be possible to run with exact conservation ($\tau = \infty$). An experiment with this choice, however, produced too much noise to be acceptable. The sensitivity of the results indicates that parts of the motion field do not fit into the advection-diffusion framework. When 2 tracers are used these motions are misinterpreted as diffusion, while when we minimize errors for 99 tracers the method will disregard the information that does not fit in. The robustness of the results with 99 tracers makes it reasonable to believe that we have isolated fundamental properties of this set of trajectories.

4.4. *Quality measure*

The crucial question is now to what extent the eddy-flux can be modelled by means of the flux-gradient formula with optimized coefficients. As a measure of how successful we have been in minimizing the errors, we have computed the correlation between real and estimated flux for the basic experiment. The fluxes have been normalized by means of $\sqrt{W_{\mathrm{vi}}}$ and $\sqrt{W_{\mathrm{wi}}}$ in the same way as in (12) and (13), and the correlation is then computed over all the 99 tracers for each grid point. Fig. 5a shows the correlation for the horizontal component of the flux. Not surprisingly, the figure shows some problems at the boundaries. There are also some areas with correlations lower than 0.9 at high levels and low latitudes. Over most of the atmosphere, however,

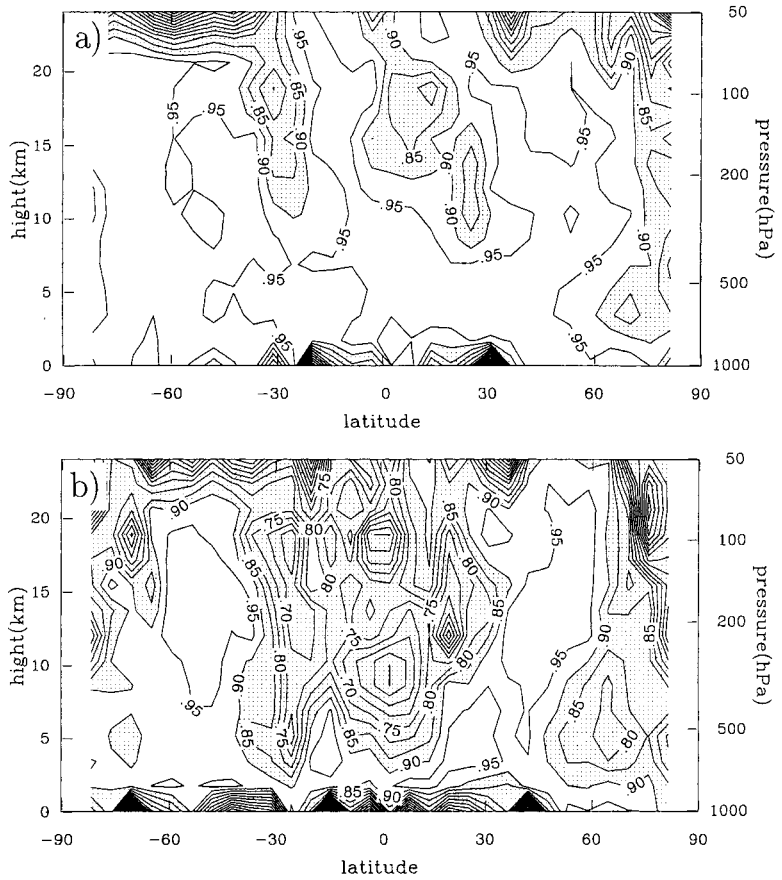

Fig. 5. (a) Correlation between $\overline{v'q'}$ and estimate based on (10) for the basic experiment. (b) Correlation between $\overline{w'q'}$ and estimate based on (11) for the basic experiment. Isoline intervals 0.05. Correlations below 0.90 are shaded.

the flux-gradient formula for this component seems to be quite successful.

Fig. 5b shows the corresponding result for the vertical flux component. Apart from boundary problems, the figure shows that something important is missing in the tropics and subtropics and also in polar regions. At the same time, however, there are also large areas where the flux-gradient formula is quite good.

5. Extended model

A natural way to try to improve the flux-gradient relation is to include terms with higher order derivatives in (10) and (11). If we go to second order we have:

$$\overline{q'v'} = -K_{yy}\frac{\partial \overline{q}}{\partial y} - K_{yz}\frac{\partial \overline{q}}{\partial z} - M_{yyy}\frac{\partial^2 \overline{q}}{\partial y^2} - M_{yyz}\frac{\partial^2 \overline{q}}{\partial y\,\partial z} - M_{yzz}\frac{\partial^2 \overline{q}}{\partial z^2}, \tag{22}$$

$$\overline{q'w'} = -K_{zy}\frac{\partial \overline{q}}{\partial y} - K_{zz}\frac{\partial \overline{q}}{\partial z} - M_{zyy}\frac{\partial^2 \overline{q}}{\partial y^2} - M_{zyz}\frac{\partial^2 \overline{q}}{\partial y\,\partial z} - M_{zzz}\frac{\partial^2 \overline{q}}{\partial z^2}. \tag{23}$$

In addition to the previous 4 coefficients we now have 6 new coefficients, denoted by M, to determine. We have done this by including the new terms in the mean square error sums (12) and

(13), and minimizing over 99 tracers. The new first-order coefficients are very similar to those of the basic experiment, and are not shown. The second-order coefficients are difficult to interpret physically, but they have a strong effect on the correlations between modelled and real flux. Fig. 6a shows that apart from some boundary problems, the horizontal flux is now well accounted for almost everywhere. Fig. 6b shows that there is also a great improvement for the vertical flux, although there are still problems in the tropical upper troposphere.

In order to find out which of the new terms that are most important we have repeated the calculation with only one new term at the time. It then turned out that most of the improvement was connected to the terms involving $\partial^2\overline{q}/\partial z^2$.

We believe that a large part of the errors of the flux-gradient approach is due to relatively simple circulation systems. Typical candidates are large, systematic circulations which take place in planes which are perpendicular to the meridional planes. These circulations will be completely masked by the zonal averaging. If they are non-random, and their size is so big that $\nabla\overline{q}$ cannot be considered as constant over a cell, they are likely to produce fluxes which will not fit into the advection-diffusion framework. The Walker circulations near the Equator are good examples of such circulations. We believe that our problems with vertical fluxes at low latitudes are to a large extent due to such circulations.

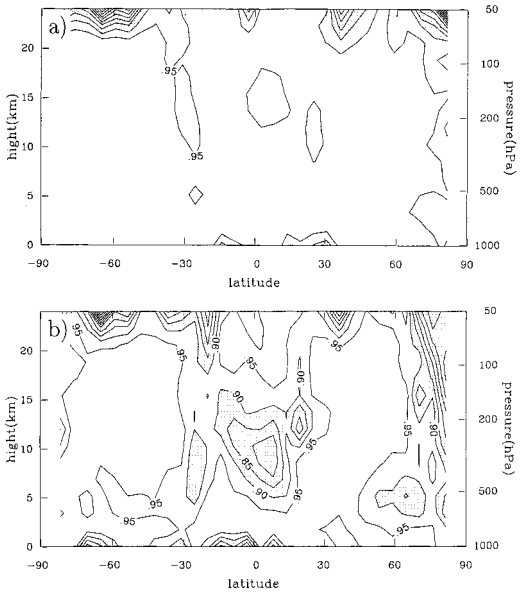

Fig. 6. (a) Correlation between $\overline{v'q'}$ and estimate based on (22). (b) Correlation between $\overline{w'q'}$ and estimate based on (23). Isoline intervals 0.05. Correlations below 0.90 are shaded.

A simple model may shed some light on the situation. Air with tracer value q_u is assumed to ascend with a vertical velocity w_u, while an equal amount of air with the value q_d is assumed to descend with vertical velocity $-w_u$. The average flux over the whole cell is then:

$$\overline{qw} = -0.5w_u(q_d - q_u). \tag{24}$$

If q_u is representative for air at a low level H_1, and q_d is representative for air at a high level H_2, then (24) can be interpreted as a flux-gradient relation. The relevant gradient, however, is not the local gradient but the average gradient over the whole depth from H_1 to H_2. The local gradient will vanish provided that q is perfectly conserved in a neighbourhood of the level where the flux is computed.

Our problems with the vertical flux at low latitudes are probably due to such phenomena where the local gradient is not appropriate. The inclusion of the second order derivative makes it possible to correct some of the errors. It is probably possible to construct even better functional relationships by including values from more levels in the formula. Related problems are encountered in connection with the atmospheric boundary layer, where K-theory is often inadequate for the modelling of convective situations. More elaborate methods based on a more general, non-local exchange between different layers have been suggested (Stull, 1988).

6. Direct method

We have also tried to compute transport velocities and diffusion coefficients directly from the trajectories without the use of tracers. In order to highlight the conceptual difficulties involved we have chosen to approach the problem in a somewhat naive way. If we focus on a point $\boldsymbol{x}_0$ fixed in space, we can study the average history of all the particles that passes through the point. For each of these particles we notice the new position $\boldsymbol{x}_+$ a

time Δt after the passage of $\boldsymbol{x}_0$. When we have done this for the whole integration period, we end up with a cloud of new positions which can be analysed with respect to mean position and spread. The velocity of the center of mass of this cloud can be estimated by:

$$\boldsymbol{v}_+ = (\overline{\boldsymbol{x}_+ - \boldsymbol{x}_0})/\Delta t\,. \tag{25}$$

In this section, the bar represents an average over all the particles involved, and the subscript + indicates that the estimate is made forward in time. The difference in (25) should not be thought of as an approximation to a derivative. If Δt goes to zero the result will be the Eulerian mean velocity, and that is not what we are searching for. Stokes drift phenomena can only be revealed by using a finite Δt larger than the period experienced by the particles when traversing the waves that are responsible for the drift. For simplicity we have chosen to attribute the velocity $\boldsymbol{v}_+$ to the position $\boldsymbol{x}_0$.

In the actual calculation we have used a procedure similar to the procedure for calculating tracer statistics. The trajectories are analysed one at the time. For each step along the trajectory we identify the closest grid point. The change in position over the interval Δt is then used to accumulate the necessary statistics as if the trajectory had passed exactly through the grid point. When all trajectories have been scanned in this way each grid point has been visited a number of times, and we can compute $\boldsymbol{v}_+$ everywhere. Zonal averaging is achieved by ignoring the longitude coordinate throughout so that the procedure becomes essentially 2-dimensional.

This zonally averaged version of $\boldsymbol{v}_+$ is related to the Lagrangian mean of Andrews and McIntyre (1978) where averages are taken over material tubes. Although no tubes occur explicitly in our procedure, we have essentially computed the average over a long succession of tubes which are released from a fixed hight and latitude and followed over a time interval Δt.

Fig. 7 shows $\boldsymbol{v}_+$ for $\Delta t = 5$ days. A striking feature is the large equatorwards velocities in the polar regions. This is not surprising considering the fact that from a starting position at the North pole one can only move southwards, never northwards. A similar phenomenon is seen near the ground where the new position $\boldsymbol{x}_+$ is more likely to be found above than below the starting position

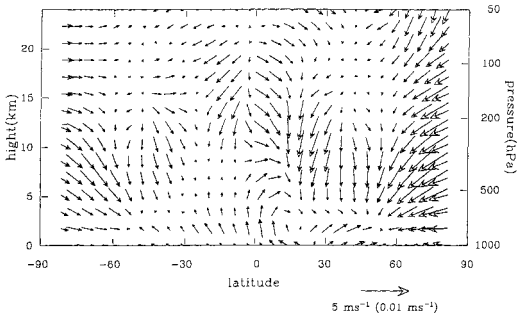

Fig. 7. $\boldsymbol{v}_+$ for $\Delta t = 5$ days.

$\boldsymbol{x}_0$. In general the the Lagrangian mean velocity defined in this way is divergent, with a tendency to be directed towards areas with stronger mixing. The reasons for this phenomenon have been discussed by Plumb (1979), Kida (1983) and Plumb and Mahlman (1987). The phenomenon also occurs in the case studies by Lyjak and Smith (1987) and Sutton (1994).

The following example may shed some more light on the issue. Consider a 2-dimensional, non-divergent, stationary flow with streamlines as illustrated in Fig. 8. The flow field is a deformation field close to a wall at $y = 0$. The figure is based on the stream function $\Psi = \mathrm{y} \sin x$ for which the problem can be studied analytically (Section 10). We shall study the set of particles with position y_0 at time t (long dashes). The line with short dashes shows the position of these particles at a later time $t + \Delta t$. The velocity component perpendicular to the wall increases away from the wall, and therefore the center of mass of this set of particles is moving away from the wall. This

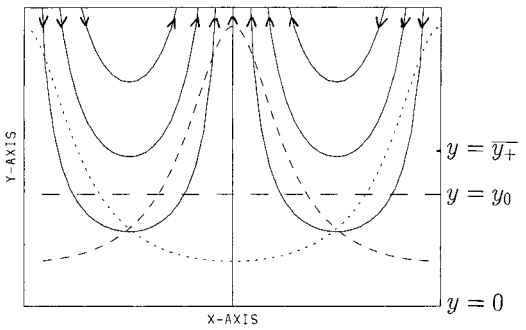

Fig. 8. Full lines: stream lines. Long dashes: string of particles at time t. Short dashes: string of particles at time $t + \Delta t$. Dotted line: string of particles at time $t - \Delta t$.

happens to any set of particles that starts out as a line parallel to the wall! However, by a similar argument we realize that before the time t, the center of mass was moving towards the wall. (The dotted line shows the position of the particles at $t-\Delta t$.) At the time t these particles are on average closer to the wall than at any other moment in their history. In this sense, we have chosen a very biased sample of particles! Clearly, the center of mass velocity depends strongly on how the particles are chosen at the beginning of the averaging interval.

Lagrangian mean velocities defined in this way suffer from the fact that they represent both mean advection and mixing. In Section 11, it is shown that for a solution to an advection-diffusion equation the center of mass velocity $\boldsymbol{v}_{\mathrm{CM}}$ is related to the mean advection $\boldsymbol{v}_{\mathrm{T}}$ and diffusivity $\boldsymbol{D}$ by:

$$\boldsymbol{v}_{\mathrm{CM}} = \boldsymbol{v}_{\mathrm{T}} + \frac{1}{\rho}\nabla\cdot(\rho\boldsymbol{D}). \tag{26}$$

The last term is due to spatial variations of the degree of mixing, and is non-divergent in the general case. Kida (1983) has argued that if the transport problem is reversed in time ($t\rightarrow -t$), the contribution from mean advection will change its sign, while the contribution from mixing will not. Thus the center of mass velocity can be split in a reversible and an irreversible part. If the example in Fig. 8 is running backwards in time we find exactly the same motion of the center of mass as in the forward case. Thus, from a zonally averaged point of view the situation is totally irreversible, and is best characterized as a kind of "mixing" with no contribution from mean advection. (This "mixing", however, is not a random process, and therefore not truly diffusive.)

In the study of GCM trajectories we can easily find the position $\boldsymbol{x}_-$ that a particle has a time Δt before it arrives in $\boldsymbol{x}_0$. This provides us with a new one-sided estimate for the center of mass velocity:

$$\boldsymbol{v}_- = (\overline{\boldsymbol{x}_0 - \boldsymbol{x}_-})/\Delta t. \tag{27}$$

Notice that $\boldsymbol{v}_-$ is equal to $-\boldsymbol{v}_+$ for the time reversed problem. When $\boldsymbol{v}_-$ is compared with $\boldsymbol{v}_+$ they turn out to be rather similar in many places, but of opposite direction indicating a large irreversible contribution. The reversible part is estimated by taking the average:

$$\boldsymbol{v}_{\mathrm{CM}} = \tfrac{1}{2}(\boldsymbol{v}_+ + \boldsymbol{v}_-) = (\overline{\boldsymbol{x}_+ - \boldsymbol{x}_-})/2\Delta t. \tag{28}$$

Notice that the difference is now centered in time, and should therefore represent a more satisfactory estimate for the center of mass velocity at $\boldsymbol{x}_0$. This velocity is shown in Fig. 9. The compensation between $\boldsymbol{v}_+$ and $\boldsymbol{v}_-$ is seen to be very strong, and most of the divergent features have disappeared. The main picture is a direct circulation extending into the extratropics of each hemisphere. This velocity is also similar to the transport velocity in Fig. 2 in that it is much weaker in the extratropics than in the tropics. The tropical circulation, however, is much weaker than for $\boldsymbol{v}_{\mathrm{T}}$. A possible explanation for this may be the considerable spatial smoothing that is expected to follow from the procedure described above. A Δt of 5 days means that the velocity of the center of mass is based on velocities spread over a large area. We have repeated the calculation for a number of different values of Δt. As expected the circulation seems to converge towards the Eulerian mean for small Δt. The strength of the tropical circulation is increased when Δt is decreased, but at the same time indirect circulations start to appear in the extratropics. Thus we have been unable and to find a Δt which produces a circulation which closely resembles the transport circulation of Fig. 2. It seems that in order to reveal the Stokes drift properly, Δt has to be chosen so large that a severe smoothing of the picture cannot be avoided. Experiments with Δt larger than 5 days show even smoother and weaker circulations than Fig. 9, and we have been unable to find any interval where the picture is independent of Δt.

In Section 11, it is shown that for an advection-

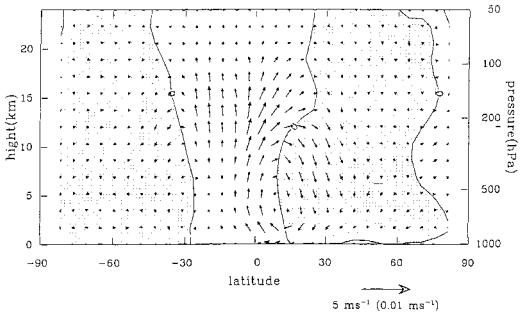

Fig. 9. As Fig. 2 but $\boldsymbol{v}_{\mathrm{CM}}$ for $\Delta t = 5$ days.

diffusion equation with constant coefficients the second order moment $\sigma_{ij}^2 = \overline{(x_i - \overline{x_i})(x_j - \overline{x_j})}$ of a cloud growing from a point is related to the diffusion coefficient D_{ij} by:

$$\frac{\partial}{\partial t}\sigma_{ij}^2 = 2D_{ij}; \tag{29}$$

Here, i and j represent coordinate directions; see also Monin and Yaglom (1977). Based on this, we have tried to estimate the diffusion coefficient by means of:

$$\boldsymbol{D}_+ = \frac{1}{2\Delta t}\overline{((\boldsymbol{x}_+ - \boldsymbol{x}_0)'(\boldsymbol{x}_+ - \boldsymbol{x}_0)'^{\mathrm{T}})}, \tag{30}$$

and also:

$$\boldsymbol{D}_- = \frac{1}{2\Delta t}\overline{((\boldsymbol{x}_0 - \boldsymbol{x}_-)'(\boldsymbol{x}_0 - \boldsymbol{x}_-)'^{\mathrm{T}})}. \tag{31}$$

Here the prime represents the deviation from the average defined above. The estimates $\boldsymbol{D}_+$ and $\boldsymbol{D}_-$ are somewhat different from each other, but both show considerable similarity to the earlier result from Fig. 1. The average of the two is even more similar to Fig. 1. However, the best correspondence with the result based on tracers was obtained with the time centered formula:

$$\boldsymbol{D}_0 = \frac{1}{4\Delta t}\overline{((\boldsymbol{x}_+ - \boldsymbol{x}_-)'(\boldsymbol{x}_+ - \boldsymbol{x}_-)'^{\mathrm{T}})}, \tag{32}$$

which is based on the spread over the interval from $t - \Delta t$ to $t + \Delta t$. Fig. 10 shows this estimate for Δt equal to 2 days. Although the picture is somewhat smoother than Fig. 1, the main maxima and minima are reproduced. In particular the very small values in the jet stream regions are verified. The tropical values of D_{0zz} are, however, much too big.

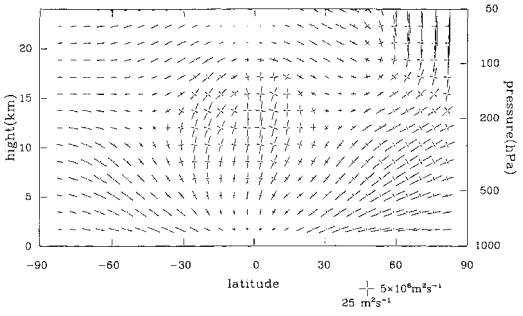

Fig. 10. As Fig. 1c but for the tensor $\boldsymbol{D}_0$ for $\Delta t = 2$ days.

When Δt is increased the picture becomes smoother and the maxima becomes weaker in most places. In the tropics, however, the component D_{0zz} increases. We believe that this is another manifestation of deep circulations of the Walker type. If a cloud of particles is growing due to random processes, the linear size of the cloud will grow like $\sqrt{\Delta t}$. Estimates based on formulas like (32) will then be independent of Δt. If the cloud is growing due to a shear in the wind field or due to the difference between rising and sinking branches of a Walker cell, then the size of the cloud will increase more like Δt itself. The corresponding coefficient estimated from (43) will then also increase like Δt. We believe that this is roughly what happens in the tropical troposphere. It is also worth noticing that whether the cloud is growing due to random processes or not, the growth is limited by the finite size of the atmosphere. Therefore coefficients based on (32) will always decrease with Δt when Δt is big enough. A similar argument applies to $\boldsymbol{v}_{\mathrm{CM}}$.

Using this direct approach it has not been possible to obtain results which are independent of the rather arbitrary parameter Δt. For this reason we consider the indirect approach with a large number of tracers to be more robust and well defined. However, we consider the results from this direct approach to be compatible with those from the tracer experiments.

7. Potential vorticity

Ertel's potential vorticity (PV) is expected to be approximately conserved for an air parcel in the free atmosphere (Hoskins et al., 1985). For this reason we have tried to estimate the eddy flux of PV by means of the flux-gradient formula (3). PV has been calculated by means of the formula:

$$Q = \rho^{-1}\left[f + \frac{1}{R\cos\phi}\left(\frac{\partial v}{\partial \lambda} - \frac{\partial u\cos\phi}{\partial \phi}\right)\right]\frac{\partial \theta}{\partial z} - \frac{\partial v}{\partial z}\frac{1}{R\cos\phi}\frac{\partial \theta}{\partial \lambda} + \frac{\partial u}{\partial z}\frac{1}{R}\frac{\partial \theta}{\partial \phi}, \tag{33}$$

which is consistent with the hydrostatic approximation. Second-order differences have been used. The eddy fluxes based on the last five months of the GCM simulation is shown in Figs. 11a and 12a. The corresponding fields computed from (3)

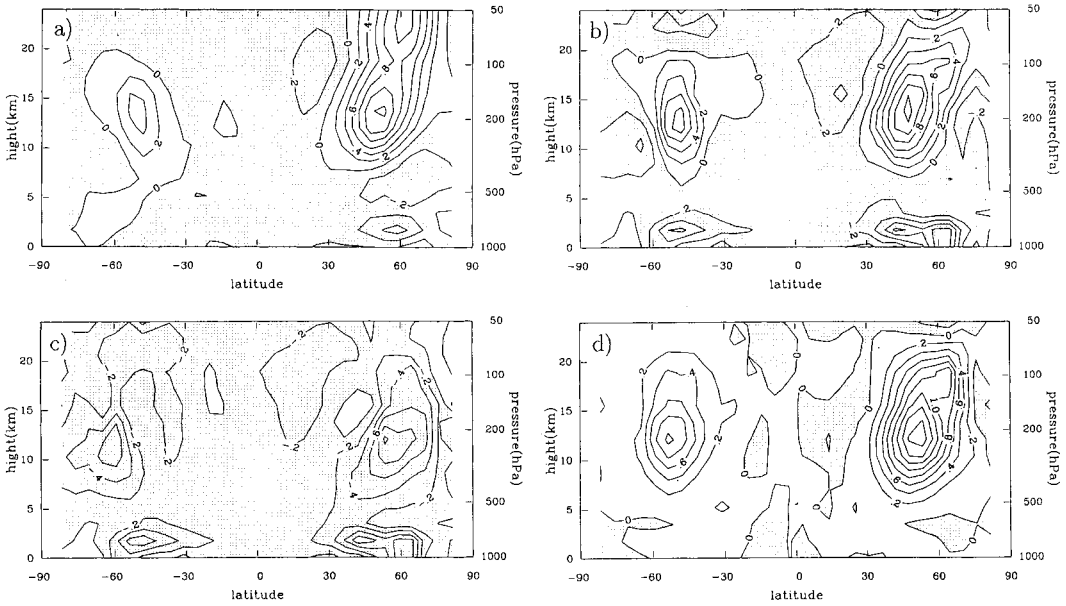

Fig. 11. (a) Horizontal eddy flux of potential vorticity $\overline{\rho v'Q'}$, units 10^{-6} K s^{-2}. (b) Same as a) but flux estimated from $-\rho \boldsymbol{K}\cdot\nabla\overline{Q}$. (c) Same as a) but flux estimated from $-\rho \boldsymbol{D}\cdot\nabla\overline{Q}$. (d) Same as a) but flux estimated from $-\rho \boldsymbol{L}\cdot\nabla\overline{Q}$.

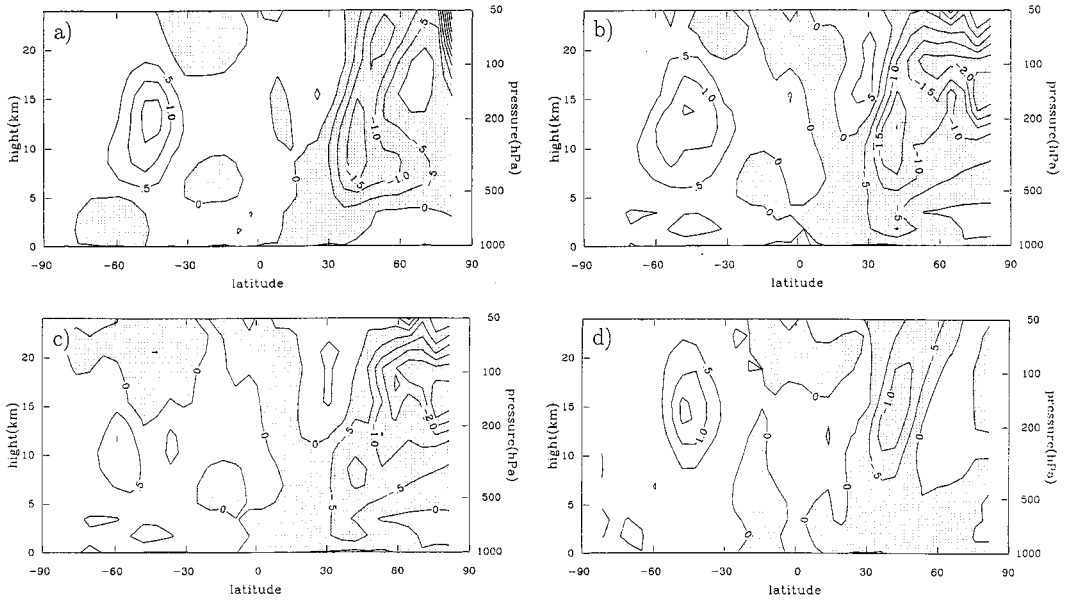

Fig. 12. (a) Vertical eddy flux of potential vorticity $\overline{\rho w'Q'}$, units 10^{-9} K s^{-2}. (b) Same as a) but flux estimated from $-\rho \boldsymbol{K}\cdot\nabla\overline{Q}$. (c) Same as a) but flux estimated from $-\rho \boldsymbol{D}\cdot\nabla\overline{Q}$. (d) Same as a) but flux estimated from $-\rho \boldsymbol{L}\cdot\nabla\overline{Q}$.

with coefficients from the basic experiment (99 tracers, $\tau = 30$ days), are shown in Figs. 11b and 12b. There is a number of reasons why we should not expect a perfect correspondence. First of all we have already demonstrated that the flux-gradient formalism has its limitations. Furthermore, PV is not a perfect tracer in the presence of friction and heat sources. Near the ground this is a serious problem, and this is probably the main reason why the flux-gradient approach is seen to fail at low levels. Due to all the derivatives PV is also a difficult parameter to deal with numerically. Our numerical formulation of (33) is not equivalent to the technique used in the model equations, and the model itself has a very low horizontal resolution (T21). For these reasons the simulated PV will not behave like a perfect tracer even when it should. Finally it is important to notice that even when PV behaves like a tracer, it is not a *passive* tracer. The velocity components appear in the the definition of PV, and information about them can be retrieved from the PV-field (the inversion principle, see Hoskins et al., 1985). Therefore the correlation between velocity and PV may not be representative for arbitrary tracers.

In light of all these remarks we find the correspondence seen in Figs. 11 and 12 quite encouraging. The discrepancies close to the ground are believed to be due to strong friction and heat sources, and also to a general problem with the numerical calculation of PV gradients close to boundaries. The last problem also exists near the poles and at high levels. In addition the errors at high levels may reflect the fact that the tracer problem used to estimate $\boldsymbol{K}$ cannot be solved properly close to the artificial open upper boundary. Between 100 hPa and 500 hPa the flux-gradient formalism seems to have caught all the main features, although the southern hemisphere maximum for the horizontal flux is too strong by a factor of two.

We have also computed the separate contributions from the symmetric (Figs. 11c and 12c) and anti-symmetric (Figs. 11d and 12d) parts of $\boldsymbol{K}$. In consideration of the weak meridional velocities outside the tropics, one might expect the contribution from mixing (symmetric part) to be dominant. This, however, is not the case. On the contrary, the two main maxima of the horizontal flux are due to the anti-symmetric part (Fig. 11d). The contribution from mixing (Fig. 11c) is seen to have the opposite sign of the total flux in most places, and is partially compensating the effect of the anti-symmetric part! In fact the horizontal flux in Fig. 11a is directed up the gradient throughout most of the atmosphere, and cannot be modelled by a diffusion term with positive diffusion coefficients. This is evident from the zonally averaged PV distribution shown in Fig. 13. The vertical flux is also seen to depend on both the symmetric and anti-symmetric contributions (Figs. 12c and d). Even if our attempt to model the PV-fluxes has only been partially successful, we feel that the correspondence is strong enough to strengthen the confidence in the parameters of the flux-gradient formula, and to demonstrate its relevance.

8. Concluding remarks

In this paper, we have tried to model the average advection of a GCM by means of a mean meridional flow together with diffusion. Several approaches have been studied. Results based on the direct calculation of mean motion and spread of particles have proved to depend heavily on the time interval used. Similarly calculations based on tracer statistics from only 2 tracers are shown to be sensitive to the relaxation which is needed. With a larger number of tracers, however, the results are rather independent of such arbitrary details of the method. Therefore we believe that the advection-diffusion operator that has been calculated represents a well defined, general property of the time dependent flow.

The advection-diffusion operator implies that we have separated the mean advection of a tracer into three different contributions; a mean circulation (transport velocity), a diffusive part, and a residual due to processes which cannot be modelled by any of the first two. We have shown that this residual is relatively small in most cases, but we have also identified some problem areas. Experiments indicate, however, that a large part of this residual can be modelled by a rather simple extension of the approach.

The transport velocity is of particular interest because it represents an alternative framework for the interpretation and modelling of eddy effects. The projection of a particle trajectory in the meridional plane can be split in two parts $\boldsymbol{x}(t) = \boldsymbol{x}_1(t) + \boldsymbol{x}_2(t)$, where $\boldsymbol{x}_1$ represents the motion due

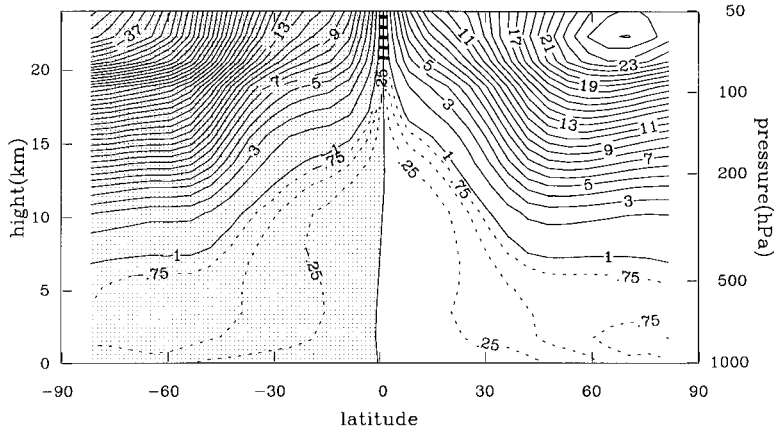

Fig. 13. Zonally averaged potential vorticity $\overline{Q}$. Units 10^{-6} m^2 K s^{-1} kg^{-1}.

to some kind of meridional circulation. If $\boldsymbol{x}_1$ is chosen to follow the Eulerian mean meridional circulation, the typical $\boldsymbol{x}_2$ will contain a systematic drift which to a large extent cancels the effect of $\boldsymbol{x}_1$ in the extratropics. This drift can be expected to disappear when $\boldsymbol{x}_1$ is forced to follow the transport velocity. Due to the way $\boldsymbol{v}_T$ is defined, the typical $\boldsymbol{x}_2$ can then be expected to be dominated by random walks and systematic oscillations about the position $\boldsymbol{x}_1$. The idea of a "true meridional circulation" is appealing, but we are not able to give a satisfactory, basic definition of such a concept. The discussion in Section 6 illustrates some of the difficulties involved. The best we can do is probably to search for the circulation (represented by $\boldsymbol{x}_1$) relative to which the "eddies" (represented by $\boldsymbol{x}_2$) attain their simplest and most random behaviour, and for this purpose the transport velocity seems to be a natural candidate. The average effect of the eddies ought to be easier to explain and model in such a framework than in a framework where $\boldsymbol{x}_2$ has a systematic drift. This will certainly be the case for conserved tracers, and it seems reasonable to expect a certain simplification also for the budgets of non-conservative quantities such as heat or momentum.

9. Acknowledgements

The GCM data set was produced by Dag Bjørge with the support of the European Centre for Medium-Range Weather Forecasts and the Norwegian Research Council.

10. Appendix A

The example in Fig. 8 is based on the stream function:

$$\Psi = y \sin x\,. \tag{34}$$

The corresponding equations

$$u = \frac{\mathrm{d}x}{\mathrm{d}y} = -\frac{\partial \Psi}{\partial y} = -\sin x\,, \tag{35}$$

and

$$v = \frac{\mathrm{d}y}{\mathrm{d}t} = \frac{\partial \Psi}{\partial x} = y \cos x \tag{36}$$

can be integrated to give:

$$\sin x = \frac{\sin x_0}{\cosh t + \cos x_0 \sinh t} \tag{37}$$

and:

$$y = y_0(\cosh t + \cos x_0 \sinh t)\,, \tag{38}$$

where (x_0, y_0) is the position at $t = 0$. The center of mass of a string of particles with constant y_0 is found by integration over x_0:

$$y_{\mathrm{cm}} = y_0 \cosh t$$

As we see, y_{cm} has its minimum for $t = 0$.

11. Appendix B

We shall now establish the connection between the parameters of an advection-diffusion formula and the behaviour of a cloud of particles. It is

convenient to write the advection-diffusion equation as

$$\frac{\partial}{\partial t}(\rho q) = -\frac{\partial}{\partial x_i}(\rho q u_i) + \frac{\partial}{\partial x_i}\left(\rho D_{ij}\frac{\partial}{\partial x_j} q\right), \qquad (40)$$

where summation over repeated subscripts is implied. We can then define an average over the tracer distribution q, and study the behaviour of various moments of this distribution. If we assume that there are no fluxes through the boundaries, the zero-order moment is independent of time, and q can be normalized so that $\int \rho q \, \mathrm{d}V = 1$. For the time derivatives of the first-order moments we then have:

$$\frac{\mathrm{d}}{\mathrm{d}t}\overline{x}_k = \frac{\mathrm{d}}{\mathrm{d}t}\int x_k \rho q \, \mathrm{d}V = \int x_k \frac{\partial}{\partial t}(\rho q)\, \mathrm{d}V. \qquad (41)$$

By means of (40) and several partial integrations we get:

$$\frac{\mathrm{d}}{\mathrm{d}t}\overline{x}_k = \overline{u}_k + \overline{\frac{1}{\rho}\frac{\partial}{\partial x_j}(\rho D_{kj})}, \qquad (42)$$

which shows how the center of mass velocity is influenced by the effect of varying diffusivity. For the second-order moments, we have:

$$\frac{\mathrm{d}}{\mathrm{d}t}\overline{x_k x_l} = \frac{\mathrm{d}}{\mathrm{d}t}\int x_k x_l \rho q \, \mathrm{d}V \qquad (43)$$
$$= \int x_k x_l \frac{\partial}{\partial t}(\rho q)\, \mathrm{d}V.$$

Again, (40) together with several partial integrations gives:

$$\frac{\mathrm{d}}{\mathrm{d}t}\overline{x_k x_l} = \overline{D}_{kl} + \overline{D}_{lk} + \overline{x_k\left(u_l + \frac{1}{\rho}\frac{\partial}{\partial x_j}\rho D_{lj}\right)} + \overline{x_l\left(u_k + \frac{1}{\rho}\frac{\partial}{\partial x_j}\rho D_{kj}\right)}. \qquad (44)$$

From (42), we have

$$\frac{\mathrm{d}}{\mathrm{d}t}\overline{x}_k\overline{x}_l = \overline{x}_k\overline{\left(u_l + \frac{1}{\rho}\frac{\partial}{\partial x_j}\rho D_{lj}\right)} + \overline{x}_l\overline{\left(u_k + \frac{1}{\rho}\frac{\partial}{\partial x_j}\rho D_{kj}\right)}. \qquad (45)$$

Subtracting this from (44), we find:

$$\frac{\mathrm{d}}{\mathrm{d}t}\overline{x'_k x'_l} = \overline{D}_{kl} + \overline{D}_{lk} + \overline{x'_k\left(u_l + \frac{1}{\rho}\frac{\partial}{\partial x_j}\rho D_{lj}\right)'} + \overline{x'_l\left(u_k + \frac{1}{\rho}\frac{\partial}{\partial x_j}\rho D_{kj}\right)'}, \qquad (46)$$

where the prime represents the deviation from the mean. Assuming D_{kl} to be symmetric, and $u_i + \rho^{-1}\,\partial/\partial x_j(\rho D_{ij})$ to be constant over the area of interest for all i, this is reduced to:

$$\frac{\mathrm{d}}{\mathrm{d}t}\overline{x'_k x'_l} = 2\overline{D}_{kl}, \qquad (47)$$

which is the relationship we have used to estimate diffusion-coefficients by means of trajectories. The last two terms in (46) describes the effect of deformation of a cloud due to gradients in the velocity field. Although we have neglected this effect in our estimates, there is no doubt that the effect may be important if the cloud is big enough.

REFERENCES

Andrews, D. G. and McIntyre, M. E. 1978. An exact theory of nonlinear waves on a Lagrangian-mean flow. *J. Fluid. Mech.* **89**, 609–646.

Hoskins, B. J., McIntyre, M. E. and Robertson, A. W. 1985. On the use and significans of isentropic potential vorticity maps. *Q. J. R. Meteorol. Soc.* **111**, 877–946.

Kida, H. 1977. A numerical investigation of the atmospheric general circulation and stratospheric-tropospheric mass exchange. I. Long-term integration of a simplified general circulation model. II. Lagrangian motion of the atmosphere. *J. Meteor. Soc. Japan* **55**, 52–88.

Kida, H. 1983. General circulation of air parcels and transport characteristics derived from a hemispheric GCM. Part 1. A determination of advective mass flow in the lower stratosphere. *J. Meteor. Soc. Japan* **61**, 171–187.

Lyjak, L. V. and Smith, A. K. 1987. Lagrangian mean circulation in the stratosphere. *J. Atmos. Sci.* **44**, 2252–2266.

Matsuno, T. 1980. Lagrangian motion of air parcels in the stratosphere in the presence of planetary waves. *Pure Appl. Geophys.* **118**, 189–216.

Monin, A. S. and Yaglom, A. M. 1971. Statistical fluid mechanics. The MIT Press, 769 pp.

Plumb, R. A. 1979. Eddy fluxes of conservative quantities by small-amplitude waves. *J. Atmos. Sci.* **36**, 1699–1704.

Plumb, R. A. and Mahlman, J. D. 1987. The zonally averaged transport characteristics of the GFDL

general circulation/transport model. *J. Atmos. Sci.* **44**, 298–327.

Sutton, R. 1994. Lagrangian flow in the middle atmosphere. Q. J. R. Meteorol. Soc. **120**, 1299–1321.

Stull, R. B. 1988. *An introduction to boundary layer meteorology*. Kluwer Academic Publishers, Boston. 666 pp.

Tibaldi, S., Palmer, T. N., Branković, Č and Cubasch, U. 1990. Extended-range predictions with ECMWF models: Influence of horizontal resolution on systematic error and forecast skill. *Q. J. R. Meteorol. Soc.* **116**, 835–866.